Sea Level and the Role of Coastal Trapped Waves in Mediating the Influence of the Open Ocean on the Coast

Chris W. Hughes[1,2] · Ichiro Fukumori[3] · Stephen M. Griffies[4] · John M. Huthnance[2] · Shoshiro Minobe[5] · Paul Spence[6] · Keith R. Thompson[7] · Anthony Wise[1,2]

Abstract

The fact that ocean currents must flow parallel to the coast leads to the dynamics of coastal sea level being quite different from the dynamics in the open ocean. The coastal influence of open-ocean dynamics (dynamics associated with forcing which occurs in deep water, beyond the continental slope) therefore involves a hand-over between the predominantly geostrophic dynamics of the interior ocean and the ageostrophic dynamics which must occur at the coast. An understanding of how this hand-over occurs can be obtained by considering the combined role of coastal trapped waves and bottom friction. We here review understanding of coastal trapped waves, which propagate cyclonically around ocean basins along the continental shelf and slope, at speeds which are fast compared to those of baroclinic planetary waves and currents in the open ocean (excluding the large-scale barotropic mode). We show that this results in coastal sea-level signals on western boundaries which, compared to the nearby open-ocean signals, are spatially smoothed, reduced in amplitude, and displaced along the coast in the direction of propagation of coastal trapped waves. The open-ocean influence on eastern boundaries is limited to signals propagating polewards from the equatorial waveguide (although a large-scale diffusive influence may also play a role). This body of work is based on linearised equations, but we also discuss the nonlinear case. We suggest that a proper consideration of nonlinear terms may be very important on western boundaries, as the competition between advection by western boundary currents and a counter-propagating influence of coastal trapped waves has the potential to lead to sharp gradients in coastal sea level where the two effects come into balance.

1 Introduction

In the open ocean, sea-level gradients [strictly, dynamic sea-level gradients as defined in Gregory et al. (this volume)] are, to first order, in geostrophic balance with currents near the surface, with wind stress adding an additional flow in the surface Ekman layer. This

---

✉ Chris W. Hughes
  cwh@liv.ac.uk

Extended author information available on the last page of the article

implies a geostrophic flow perpendicular to the sea-level gradient. The mean ocean currents sustain sea-level differences of around 3 m between the North Pacific subtropical gyre and the Weddell Sea near Antarctica (Rio et al. 2014).

If sea level slopes along the coast, the implied geostrophic flow is towards or away from the coast, inconsistent with the coastal boundary condition of no normal flow. Thus, as the coast is approached, a different dynamical balance must come into play. This change in dynamical balance has, in many cases, the effect of reducing the size of the signal, so that sea-level changes at the coast can be smaller than nearby open-ocean changes.

When a change of forcing occurs on the ocean, the oceanic response to that change can be felt at distant locations after some time. This information transfer happens in part because of advection by ocean currents, but usually the fastest response is mediated by waves. Thus waves, and in particular those in the coastal waveguide, known as coastal trapped waves (CTWs), play an important role in setting up the coastal sea-level response to open-ocean changes. In this paper, we focus on the way in which an understanding of CTWs informs the interpretation of this coastal response. We will find that, for continental boundaries, the strong mesoscale variability in the ocean interior is strongly damped at the coast, meaning the basin-scale signals are the main consideration. We start here by summarising elements of wave phenomenology, identifying salient features to be described in more detail later in this paper.

1.1 Waves in a Flat-Bottom Ocean

In idealised models of the ocean with a flat bottom and vertical sidewalls, linear ocean waves can be sorted into orthogonal vertical modes with different vertical structures. These modes are enumerated by the number of vertical nodes (i.e., depths at which the amplitude is zero). For each mode of subinertial frequency (wave frequency σ less than f or periods longer than the inertial period of $2\pi/f$, where f is the Coriolis parameter), the waves can be classified as Rossby waves in the interior (arising from meridional gradients in the Coriolis parameter), and Kelvin waves at the boundary. Rossby waves have westward phase speeds, yet only long Rossby waves (whose wavelength is longer than 2π times the Rossby deformation radius) have westward group velocity whereas shorter Rossby waves have eastward group velocity. Superinertial waves (waves with frequencies greater than f and periods less than $2\pi/f$) are characterised differently. For this review, we focus on the subinertial regime for which coastal trapping is possible.

Kelvin waves are a form of CTW, with the Rossby deformation radius acting as an exponential decay scale away from the vertical side boundary. Kelvin waves propagate cyclonically around an ocean basin with the boundary on the right (facing in the direction of propagation) in the northern hemisphere and on the left in the southern hemisphere. They also generally move much faster than Rossby waves of the corresponding mode. In particular, Rossby waves travel fastest at the equator, at one third of the equatorial Kelvin wave speed, and they slow dramatically with increasing latitude whereas Kelvin waves do not. This contrast is illustrated for the first baroclinic mode (mode-1) in Fig. 1.

Mode-0 waves (the barotropic mode) adjust rapidly, with the Kelvin wave speed being of order 200 m s^{-1} and the Rossby radius of order 2000 km. Consequently, Mode-0 Kelvin waves transfer forcing change information globally in just a few days (Lorbacher et al. 2012). For higher wave modes, the adjustment time scale can be much longer. The Mode-1 (first baroclinic) equatorial Kelvin wave speed is typically 2.5 m s^{-1}. Furthermore, the corresponding Mode-1 Rossby-wave speed drops below 10 cm s^{-1} poleward of about 20°,
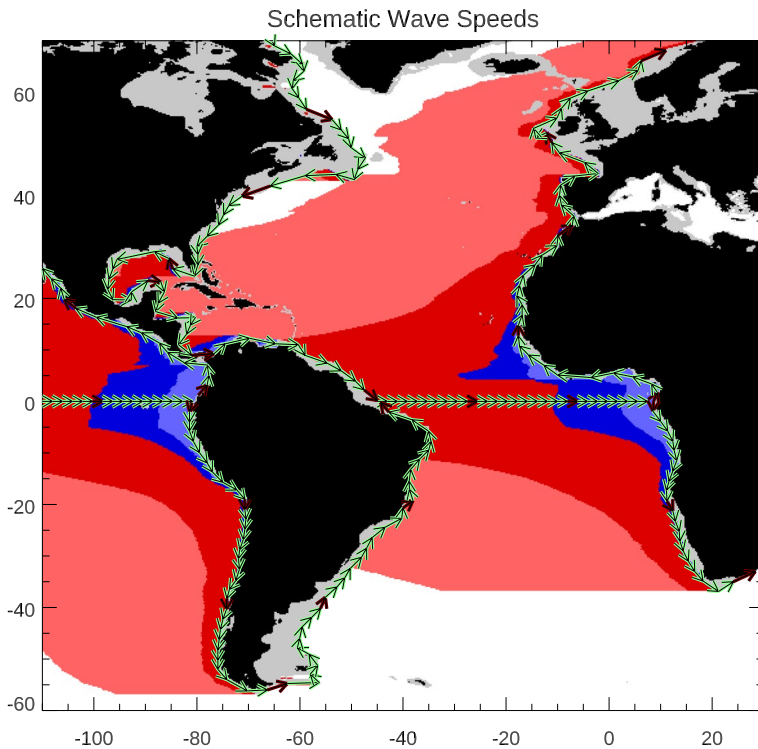
Fig. 1 Illustration of subinertial wave speeds in a flat-bottomed ocean, showing the fastest (long wavelength) mode-1 waves, and assuming a spatially uniform typical Kelvin wave speed of 2.5 m s^{-1}. Arrows show the distance covered per day by Kelvin waves, with every tenth day highlighted. Colours show the westward distance covered by Rossby waves from the eastern boundary in ten days (pale blue), one month (dark blue), one year (red) and ten years (light red). For each, the boundary of the ocean is taken as the 500 m isobath (shallower regions are grey). In a more realistic ocean with variable stratification and bathymetry, the Rossby-wave speeds would be reduced, and the boundary wave speeds increased, at high latitudes

with theoretical speeds below 1 cm s^{-1} poleward of about 60° (Chelton and Schlax 1996). The ocean, of course, does not have a flat bottom. Away from the continental slopes, even the relatively weakly sloping seafloor has an influence on the structure of Rossby waves, strongly reducing the amplitude of the Mode-1 Rossby wave at the seafloor and slightly altering its dispersion relation, but otherwise the general results from flat-bottom theory remain valuable (LaCasce 2017).

1.2 The Disparity Between Coastal and Open-Ocean Wave Speeds

There is a great disparity in wave speeds and length scales between coastal signals and open-ocean signals. The open-ocean adjustment process is dominated by basin-scale Rossby waves, whereas boundary waves are trapped to the continental slope over a length scale that is the larger of the Rossby radius (in the case of a Kelvin wave) and the width of the slope itself (as we will see for other kinds of coastal trapped waves). This length scale is typically tens of kilometres outside the tropics, and a maximum of about 250 km near

the equator (excluding the rapidly adjusting mode-0, which is basin scale). Within a few equatorial Rossby radii of the equator, equatorial Kelvin waves and Yanai waves (mixed Rossby-gravity waves) carry signals rapidly to the east, thus removing the coastal trapping found away from the equator. The above dynamics is standard and is described in oceanography textbooks such as that of Gill (1982).

The disparity in wave properties means that the coast is a special place, with communication of signals along the coastal boundary moving rapidly compared to the ocean interior. There is hence the possibility of a decoupling between coastal and open-ocean sea-level signals. Such a decoupling is seen in observations and ocean models, which show quite different spectra of sea level between the coast and the open ocean in many regions, though most dramatically away from the equatorial and eastern boundary regions (Hughes and Williams 2010; Bingham and Hughes 2012; Hughes et al. 2018).

The effect of rapid propagation of coastal trapped waves is seen in the coastal sea-level response to El Niño events along the eastern boundary of the Pacific (Enfield and Allen 1980; Kurapov et al. 2017). It has also been noted indirectly via the uniformity of sea-level signals around Antarctica as discussed by Hughes et al. (2014) and references therein, and by an analogous mode in the Arctic (see Fukumori et al. 2015 and references therein). These polar modes are manifestations of the response to near-coastal winds being trapped and rapidly propagated along the coast, a phenomenon also seen in the eastern North Atlantic (Calafat et al. 2012, 2013), and discussed in more detail elsewhere in this volume. Further indirect evidence of the influence of CTWs is seen in the coherence of sea-level signals above long stretches of the global continental slope (Hughes and Meredith 2006). Recent model-based analysis suggests that much of the shelf coherence results from the strong suppression of mesoscale variability over the continental slope, thus permitting the large-scale barotropic mode to be seen in the resulting quiet regions (Hughes et al. 2018), representing an indirect manifestation of CTW effects.

1.3 Importance of the Continental Slope

The influence of the continental slope on the results described above highlights an important aspect of the real ocean, namely it does not have vertical sidewalls. Instead, as illustrated in Fig. 2, typical offshore bathymetry at the coast consists of a gently sloping shelf
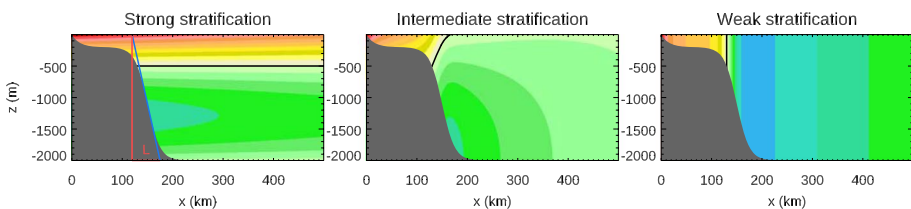

Fig. 2 Schematic showing the typical configuration of topography, coordinate system, and mode-1 CTW characteristics for various strengths of stratification as defined by the Burger number (see text). The y direction is into the page and would be to the north if the boundary is on the west of the ocean. Grey shading represents topography, with a typical gently sloping shelf region, followed by a steeply sloping continental slope. The topographic length scale L corresponding to a particular position (where the blue line is tangent to the slope) is illustrated in the first panel. Shading represents the perturbation pressure associated with the mode, with the node (zero value) marked with a black contour. In the northern hemisphere, the wave would be propagating out of the page (the opposite in the southern hemisphere). The offshore decay in the strong stratification case is exaggerated, to make it more visible

region, followed by a steeply sloping continental slope down to the abyssal plain of the open ocean. In the presence of a sloping sidewall, CTWs are no longer pure Kelvin waves. Given that the rapid propagation of CTWs appears to be responsible for the above-mentioned decoupling between the coast and open ocean, we assume that physical characteristics of CTWs play an important role in mediating the influence of the open ocean on the coastal region. The purpose of this paper is to review the extent to which this assumption offers a valuable framework for understanding how the open-ocean communicates with the coast. We begin by considering properties of CTWs when sloping topography is present. The complementary question of how CTWs act to trap and propagate sea-level signals that are themselves generated close to the coast, rather than in the open ocean, is considered elsewhere in this volume.

At subinertial frequencies, and assuming f to be constant (the f-plane approximation is almost ubiquitous in the theory of CTWs; this is a significant issue which we will pick up later on), it remains the case even with nontrivial topography that plane waves cannot propagate away from the shore. There are still waves that travel along-shelf with an off-shelf decay. Hence, the concept of CTWs remains valid. However, the presence of topography breaks the decomposition into vertical modes. Typically, these CTWs form a sequence with an increasing number of nodes in bottom pressure, spaced down the slope, as we see in baroclinic Kevin waves for the vertical sidewall case. What is different is that the nodes reach the sea floor at different distances from the shore, because of the finite slope, and their extension away from the sea floor is no longer horizontal as it is in baroclinic Kelvin waves, but at some angle, becoming vertical in the barotropic limit (Huthnance 1978), as seen in Fig. 2.

For a given along-shelf wavelength, higher modes (with more offshore nodes) have lower frequency and propagate more slowly. Mode-0, which depends on the surface of the ocean being free to move (i.e., not rigid) is termed a (barotropic) Kelvin wave. Even in the presence of topography, the mode-0 Kelvin wave usually has maximum elevation at the coast and offshore decay with no change of sign and is much like the barotropic Kelvin wave in the flat-bottom case. Typically mode-1 also has maximum elevation at the coast and a node near the shelf break. As the forms with simplest and largest-scale spatial structure (shelf-width scale for mode-1) modes 0 and 1 are most naturally generated by large-scale forcing (from atmosphere, deep ocean or tides) with resulting maximal effects of elevation at the coast. Along-shelf phase propagation remains cyclonic around an ocean basin with typical speeds of hundreds of metres per second for a mode-0 Kelvin wave and several metres per second for mode-1. The speeds other than mode-0 tend to be similar to, or faster than, the corresponding pure (i.e., vertical sidewall) baroclinic Kelvin wave speeds.

2 Properties of f-plane Coastal Trapped Waves

CTWs are subinertial waves (wave frequency σ less than the magnitude of the inertial frequency $|f|$), with along-shelf propagation and off-shelf decay. We here present a summary of their properties on the f-plane. Far more details, including mathematical derivations, can be found in the review papers by Huthnance (1978), Mysak (1980a), Mysak (1980b), Huthnance et al. (1986), Huthnance (2001) and references therein. We follow the usual convention whereby the waves are described using a coordinate system with $\hat{\mathbf{x}}$ (the unit vector along the x-axis) pointing in the off-shelf direction into the ocean interior (as in Fig. 2) and the y-axis direction, $\hat{\mathbf{y}}$, directed along the coast (pointing

into the page in Fig. 2). Hence, northern hemisphere waves propagate in the $-\hat{\mathbf{y}}$ direction for a right-handed coordinate system in which $\hat{\mathbf{z}}$ points upwards (note that $\hat{\mathbf{y}}$ points approximately to the north on western ocean boundaries, and to the south on eastern boundaries).

We are concerned with the following restoring mechanisms leading to ocean wave propagation: gravity (tending to level the sea surface and interior isopycnals; the Kelvin wave mechanism) and potential vorticity conservation (tending to constrain any bottom-reaching flow to be along depth contours in the f-plane limit). The latter is analogous to the Rossby-wave mechanism that gives westward phase propagation in the open ocean due to the meridional gradient of the Coriolis parameter. We thus refer to "topographic Rossby waves" when the potential vorticity gradient is predominantly due to gradients in water depth (i.e., topographic β), rather than gradients in the Coriolis parameter (planetary β). In this manner, cyclonic around an ocean basin corresponds to the westward phase propagation of Rossby waves. Another common term for CTWs, especially in the unstratified case, is "continental shelf waves".

The two relevant length scales are the cross-shelf scale of the topography, L, and the first baroclinic Rossby deformation radius, L_d. The cross-shelf length scale is given by $L = h/|s|$, where $z = -h(x, y)$ is the vertical position of the ocean bottom topography and $s = \partial h / \partial x$ is its offshore slope. The deformation radius L_d scales approximately as $NH/|f|$ where H is the vertical scale and N is the buoyancy frequency measuring the strength of stratification: $N^2 \equiv -(g/\rho_0)\mathrm{d}\rho/\mathrm{d}z$ where z is the vertical coordinate (positive upward), g is acceleration due to gravity, $\rho(z)$ is the background vertical structure of potential density at rest and ρ_0 is a reference background density. When stratification is strong, i.e., the Rossby radius of deformation exceeds the cross-shelf topographic scale, the continental slope and shelf may be "seen" by the wave as a near-vertical sidewall. Waveforms in this limit are modes of vertical structure with off-shelf decay on the scale of the Rossby radius of deformation, i.e., they act like "Kelvin waves". Strong stratification corresponds to a narrow shelf slope compared to the Rossby radius: $(L_d/L)^2 \gg 1$. Here, $(L_d/L)^2$ is approximately equivalent to the Burger number

$$S \equiv N^2 H^2 / f^2 L^2 \approx (L_d/L)^2. \tag{1}$$

The spatial structure of a wave mode changes as stratification, topography and/or latitude changes. Nodal lines of perturbation pressure typically tilt upward towards the surface, from horizontal (strong stratification/steep topography/low latitude, $S \gg 1$) in the Kelvin wave limit to vertical (weak stratification/broad topography/high latitude, $S \ll 1$) in the barotropic topographic Rossby-wave limit. Figure 2 schematically illustrates the progression from strong-to-weak stratification for mode-1, with the nodal lines marked in black. In the Kelvin wave limit, the modes have the same offshore structure as the corresponding open-ocean vertical modes. As stratification weakens, the slope becomes less steep, or $|f|$ increases, the CTW modes evolve more complex structures which no longer match the interior modes, and are not separable in the vertical coordinate, until they become simply barotropic in the low S limit. A clear example of this transformation of modal structure from equator to high latitude is given by Allen and Romea (1980), who also explain how (in the absence of scattering by small-scale topography) energy is retained within a particular mode even as its structure changes with latitude.

2.1 Characteristic Properties in Various Limits

For mode-1 in the relatively weak stratification limit (i.e., a topographic Rossby wave or "continental shelf wave"), the cross-shelf scale tends to match the shelf width L. At low frequencies, the waves become nondispersive with a propagation speed of order Lf, which is $\mathcal{O}(10 \text{ m s}^{-1})$ for $f = 10^{-4} \text{ s}^{-1}$, $L = 100$ km. Hence, long period implies long wavelength. Mode-1 tends to have a maximum (subinertial) frequency at which the along-shelf scale is comparable with the shelf width. Shorter waves then have lower frequency so that energy propagation at the group velocity is reversed (phase propagation remains cyclonic around the deep ocean). This behaviour is again analogous to Rossby waves: the frequency maximum for Rossby waves is at a length scale (wavelength divided by 2π) which is comparable to the smaller of the Rossby radius and the meridional length scale, whereas for CTWs the frequency maximum is at a length scale comparable to the shelf width. As the stratification increases, the waves transition towards (internal) Kelvin waves with a propagation speed of order NH, which is $\mathcal{O}(1 \text{ m s}^{-1})$ for a bottom-top density difference $0.001\rho_0$ in depth 100 m. Correspondingly, for stratification-dominated waves (the Kelvin wave limit) the dispersion relation for frequency σ as a function of along-slope wavenumber k can approach and even pass smoothly through the inertial frequency as k increases (Dale et al. 2001).

For short along-slope wavelengths (large k), the general coastal trapped wave form is bottom trapped. Bottom-trapped waves (Rhines 1970) are a limiting case in simple geometry, with uniform stratification N^2 and motion everywhere parallel to a plane sloping seafloor; they decay away from the seafloor. They can propagate up or down the slope, but always with a component along the slope cyclonically around the deeper water. In more general geometries, CTWs in the large k limit become bottom-trapped waves confined near the seafloor where Ns is maximum, with frequency given by $\sigma = Ns$ (Huthnance 1978).

With increasing distance from the equator, the inertial frequency f increases from zero in proportion to the sine of latitude. Oceanic stratification also generally decreases. For any given offshore profile of coastal bathymetry, these changes imply a poleward trend from more to less stratification (decreasing Rossby radius of deformation or decreasing Burger number). This transition of the Burger number thus leads to a transition from (internal) Kelvin waves towards topographic Rossby waves. An implicit assumption is that changes in f, the stratification, and the continental shelf form are small over one wavelength, so that local wave forms are roughly as for a uniform shelf. Then also individual wave modes conserve along-shelf energy flux. However, in realistic cases the shelf-depth profile can vary relatively rapidly, thus causing scattering between wave modes.

The shelf width may be the most important factor in determining whether stratification is "strong", i.e., if the Rossby radius of deformation exceeds the cross-shelf scale L so that the Burger number is larger than unity. With a bottom-top density difference of $0.001\rho_0$, $f = 10^{-4}\text{s}^{-1}$ and $L = 100$ km, the Burger number is $S = 10^{-4}H$ where H is the water depth measured in metres. For this case with a fairly wide shelf, stratification is weak, especially over the shelf where H is small. For a narrower shelf of $L = 10$ km, then $S = 10^{-2}H$ (again, with H in metres). In this case, stratification is strong especially over the adjacent slope. At a latitude of about 12.5° the factor f^{-2} in S becomes ten times larger than the typical midlatitude value of f assumed above, thus making stratification ten times more effective than in the above scalings.

2.2 The Long-Wave Limit

The long-wave limit is (as we will show below) the most relevant to open-ocean interaction with the coast at periods longer than a few days. At very low frequencies and negligible bottom friction, with correspondingly small along-shelf wavenumber, and with shelf-width scales much smaller than the barotropic Rossby radius ($gH/f^2L^2 \gg 1$), we use the linear, inviscid boundary equations:

$$\rho_0 f v' = \frac{\partial p'}{\partial x}, \tag{2}$$

$$\rho_0 \frac{\partial v'}{\partial t} + \rho_0 f u' = -\frac{\partial p'}{\partial y}, \tag{3}$$

$$\rho_0 \frac{\partial \rho'}{\partial t} + \rho_0 \frac{N^2}{g} w' = 0, \tag{4}$$

where primes represent perturbations about a stably stratified state of rest. Assuming a wave-like form travelling along the boundary, with $(u', v', w', \rho', p') = (u, v, w, \rho, p)e^{i(ky-\sigma t)}$, and substituting into the momentum equations, we find that velocity components are related to pressure p by

$$\rho_0 f^2 (u, v) = \left(-ik \left[-c \frac{\partial p}{\partial x} + fp \right], f \frac{\partial p}{\partial x} \right). \tag{5}$$

Here we are assuming a wave propagating in the y direction (along-slope). This means that the wave phase speed is $c = \sigma/k$ (we will find that c takes the opposite sign to f), and imaginary quantities are 90° out of phase with real quantities. Thus along-shelf flow v is in phase with the pressure field, but cross-shelf flow u lags it by 90°. Within Eq. (5), the pressure p obeys

$$\frac{\partial^2 p}{\partial x^2} + \frac{f^2}{N^2} \frac{\partial^2 p}{\partial z^2} = 0. \tag{6}$$

The boundary condition of no normal flow through the seafloor $w = -u\mathrm{d}h/\mathrm{d}x$ at $z = -h(x)$ means that at the bottom we have

$$\frac{\partial h}{\partial x} \left(\frac{\partial p}{\partial z} - \frac{fp}{c} \right) + \frac{f^2}{N^2} \frac{\partial p}{\partial z} = 0. \tag{7}$$

Assuming a rigid lid boundary condition, which is usually a good approximation for modes 1 and higher, but not the mode-0 Kelvin wave, the equivalent boundary condition at the top is

$$\frac{\partial p}{\partial z} = 0. \tag{8}$$

Since only c appears in Eq. (7), rather than σ and k separately, the eigenmodes that satisfy Eq. (6) and its boundary condition all have the same speed c for all wavelengths in this long wavelength limit. This means that long waves are nondispersive and characterised by a single propagation speed for each mode.

Given speeds measured in metres per second (hundreds of kilometres per day), these long waves are clearly the appropriate limit for considering the coastal influence of open-ocean currents with natural time scales of more than a few days. However, as time scales become longer, it becomes important to consider the role of friction.

Friction causes cross-shelf phase shifts, altered amplitude distributions, and significant damping of CTWs (e.g., Brink 1982, 1991). Qualitatively, this effect can be understood by thinking in terms of how the ocean responds to an externally imposed along-shelf wind stress τ rather than the along-shelf pressure gradient which is a part of the wave itself. For idealised uniform conditions (no along-shelf pressure gradient and no on-offshore transport), the depth-integrated alongshore momentum balance is

$$\partial v/\partial t + rv/h = \tau/\rho_0 h. \tag{9}$$

In this equation, v is the along-shelf component of flow and r is a bottom friction coefficient with units of speed. This friction coefficient expresses a linear drag law proportional to bottom velocity, based on an assumed quadratic drag linearised around a background, usually tidal velocity u_0. The momentum equation (9) means that the along-shelf flow is in phase with the forcing wind stress τ if the frequency of oscillation of the stress is much smaller than r/h (in which case the time tendency term can be dropped). In contrast, the flow lags more as the frequency increases to approach r/h. Since drag becomes important more rapidly (i.e., at higher frequency) in shallower water, its effect is to bias v to greater amplitude in deeper water, which in turn mitigates the damping effect (Huthnance 2001). For example, nearshore currents lag the wind less than currents in deeper water offshore. Within damped CTWs, it is found that v shifts from being in a geostrophic balance $v \propto \partial p/\partial x$ offshore (where h is large) to a frictional balance in which flow is down the slope of sea level $v \propto \partial p/\partial y$ in shallow water.

Damping rates may be estimated as $r/h = \mathcal{O}(0.003\,u_0\,h^{-1})$, where the value 0.003 is a standard non-dimensional quadratic drag coefficient. This leads to a decay time less than 4 days for a typical current with $u_0 = 0.1$ m s^{-1} and depth $h = 100$ m. This decay time converts to a decay distance $c_g h/r$ for a wave with energy propagation speed c_g. Such decay distances are largest (hundreds to a thousand kilometres or more) for long waves with 'forward' energy propagation; much less for (short) waves with slow 'backward' energy propagation.

Thus, although CTWs are an important factor in regulating the link between the ocean and coast, for time scales of days and longer it is important to include the role of friction. In order to understand this effect in more detail, we reintroduce bottom drag and consider the low frequency limit for which the coastal adjustment to open-ocean changes may be considered to be complete, and a steady state has been reached.

2.3 The Low Frequency Limit

We now examine how variability on the middle and outer shelf can influence coastal sea level as $\sigma \rightarrow 0$, remaining on an f-plane, showing that the effect of the continental slope is to smooth the open-ocean sea-level signal, and shift it in the direction of CTWs before it reaches the coast.

To simplify the discussion, we follow Csanady (1982) and references therein, and assume a straight coast at $x = 0$ and a "wedge" depth profile of the form $h = sx$ defined over a coastal strip of width l. The flow is assumed to be steady, linear and barotropic and the wind stress is zero. A further simplification (which results from the along-shelf

currents being much larger than the cross-shelf currents) is the neglect of bottom stress in the cross-shelf direction leaving a geostrophically balanced alongshore flow.

Under the above assumptions, the sea-level distribution over the coastal strip ($0 < x < l$) satisfies

$$\frac{\partial \eta}{\partial y} = -\frac{r}{fs}\frac{\partial^2 \eta}{\partial x^2}. \tag{10}$$

As noted by Csanady (1978), this is a diffusion equation with alongshore distance in the direction of CTW propagation playing the role of time. The coastal boundary condition of no normal flow, combined with the alongshore momentum balance as depth tends to zero, leads to a boundary condition $\partial \eta / \partial x = 0$ under the present assumptions. The offshore boundary condition specifies $\eta(l, y)$.

This highly idealised model illustrates two important consequences of the coastal boundary condition. First, spatial variations of mean sea level "diffuse" along the coastal strip in the same direction as CTW propagation, i.e., cyclonically. This feature explains the use of "Arrested Topographic Wave" to describe Csanady's model. Second, this diffusive effect leads to coastal sea level being smoother than the variability offshore. More specifically, if the sea level at the offshore boundary of the coastal strip is taken to be $\eta(l, y) = \cos(ky)$ then sea level at the coast is given by $A(k)\cos(ky + \phi)$ where the gain $A(k) \to 1$ from below as $k \to 0$; only infinite wavelengths diffuse completely to the coast (Fig. 3).

A more complete analysis includes the effect of stratification (Huthnance 2004). Consistent with the above discussion it is concluded that coastal tide gauges can only monitor large-scale oceanic motion with scales of thousands of kilometres. Lin et al. (2015) provide observational evidence for the smoothness of mean sea level along extended coastlines exposed to the open ocean. Based on an analysis of mean sea level observed by 31 tide gauges along west coast of North America, and a realistic model of the geoid, they showed that changes of coastal mean sea level have a range of about 0.3 m between 30 and 60°N. They then used the Arrested Topographic Wave model to show that the primary driver of this alongshore variability was wind forcing over the shelf rather than the open ocean, consistent with simulations by realistic ocean models.

On other coastlines, however, different dynamics apply. Tide gauge data, satellite altimetry, and ocean model simulations agree on the general features of the global coastal mean dynamic topography (Woodworth et al. 2012; Andersen et al. 2018), which shows smooth variations on eastern boundaries (except at the Strait of Gibraltar where the Mediterranean inflow allows for a step, Hughes et al. 2015), but larger and sharper steps in places along western boundaries, with different models in particular showing significant differences in the latter case. The sharp steps appear to be associated with western boundary currents, the Gulf Stream in particular being a clear example (Higginson et al. 2015), but the steps are smaller than those across the western boundary currents and occur equatorward of the main open-ocean step as if displaced in the direction of CTW propagation.

In summary, the coastal boundary condition of no normal flow has a profound influence on the way signals originating in the open ocean are transmitted across the shelf to the coast: spatially smoothing the ocean signal and diffusing it along the shelf in the same direction as CTW propagation. It is important to note, however, that the Arrested Topographic Wave model is only relevant on the inner shelf and describes how sea-level variability on the middle to outer shelf is transmitted to the coast. It is not meant to model the transmission of signals across the slope to the open ocean. We return to this more complicated problem in Sect. 3.
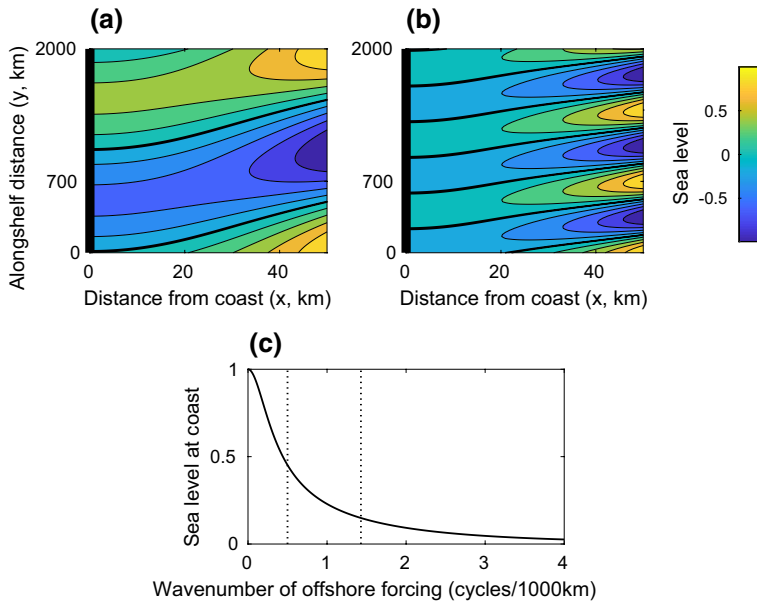
Fig. 3 Response of coastal sea level to steady sinusoidal forcing specified at the offshore boundary of a narrow coastal strip, calculated using Csanady's Arrested Topographic Wave model (see text for details). **a**, **b** Sea level as a function of cross (x) and along (y) shore distance. The coast is at $x = 0$ and marked by the thick black vertical line. The offshore boundary is at $x = 50$ km where sea level is assumed to be sinusoidal with unit amplitude and alongshore wavelength of **a** 2000 km and **b** 700 km. Zero contours are shown by the thicker black lines. **c** The amplitude of coastal sea level as a function of the wavenumber of the offshore forcing. The wavenumbers used in **a** and **b** are indicated by the dotted lines. The linear friction coefficient is 5×10^{-4} m s^{-1}, the Coriolis parameter is 10^{-4} s^{-1} and the slope of the wedge-shaped bathymetry is 3×10^{-3} (implying a depth of 150 m at the offshore boundary)

Given the apparent importance of bottom friction in allowing the ocean sea-level signal to "diffuse" towards the coast, we now consider the possibility of dynamical effects that may reduce the role of bottom friction.

2.4 Slippery Bottom Boundaries

It has been pointed out (MacCready and Rhines 1993 and references therein) that the presence of stratification can have an important effect on the operation of bottom friction. Friction induced by a bottom current along isobaths will result in an Ekman flux perpendicular to those isobaths, advecting buoyancy up or down the slope. The resulting upwelling or downwelling leads to horizontal density gradients near the bottom which in turn produce a change in the bottom geostrophic flow, as a result of the associated change in thermal wind balance. The result is always a tendency to reduce the near-bottom geostrophic flow, and hence reduce the friction, thus making the bottom effectively more "slippery" than might initially be thought (although the flow near the bottom has been reduced, this Ekman flux-induced adjustment means the frictional interaction of the flow with the bottom is subsequently reduced). In fact, a similar process applies over a flat bottom, as a result of the convergence or divergence of the Ekman flux, but the presence of a slope can accelerate the process as it does not require the Ekman flux to be divergent.

The logical extreme of this idea is that, after some time, the bottom geostrophic flow tends to zero and bottom friction ceases to act at all. It is important to put this interpretation into a broader context to see why it cannot be correct in general, though there are circumstances in which it may be a useful concept.

First, in the context set out by MacCready and Rhines (1993), the bottom geostrophic flow does not decay to zero, but to a particular value determined by a balance between vertical diffusion and upslope Ekman flux of density. It could only approach zero in the absence of diffusivity. Furthermore, diffusion is the only form of forcing in this scenario, as the problem considered involves no wind stress and no influence from the open ocean (which we will discuss below in terms of the addition of varying Coriolis parameter) other than the establishment of a background stratification.

Second, if we consider the steady, linear, along-slope, depth-integrated momentum budget, as there is no variation in depth in the along-slope direction, bottom form stress does not appear and the budget can be written as

$$fU = -\frac{\partial P}{\partial y} + \tau_{\mathrm{s}} - \tau_{\mathrm{b}}, \tag{11}$$

where U is the depth-integrated offshore mass transport, P is the depth-integrated pressure, τ_{s} is the alongshore surface wind stress, and τ_{b} is the alongshore stress on the bottom. The terms on the right-hand side represent the offshore geostrophic, wind-driven Ekman, and bottom Ekman flows, respectively. As the depth approaches zero at the coast, both U and P must approach zero, being depth integrals of finite quantities, so the balance becomes one between wind stress and bottom stress, meaning that bottom friction cannot reduce to zero. This is consistent with the steady-state form of Eq. (10) in Sect. 2.3 describing the Arrested Topographic Wave: in the absence of wind stress, the bottom stress must decay to zero at the coast, but balance the depth-integrated pressure gradient offshore.

Third, if we take the curl of the steady, depth-integrated linear momentum equations (e.g., substitute constant f, $H = h(x)$, $Q = 0$ and $\partial/\partial t = 0$ into equation 20 of Hughes 2008), then we obtain

$$\frac{\partial p_{\mathrm{b}}}{\partial y}\frac{\mathrm{d}h}{\mathrm{d}x} = \hat{\boldsymbol{k}} \cdot \nabla \times \boldsymbol{\tau}, \tag{12}$$

where p_{b} is the bottom pressure and $\boldsymbol{\tau}$ is the vector surface minus bottom stress. In this equation, we have ignored nonlinear terms in the momentum equation and the very small effect of stress due to atmospheric pressure acting on the free surface slope of the ocean, but otherwise the equation is general and applies in either stratified or unstratified oceans. Integrating along characteristics (contours of h in this case) shows that, in the absence of any bottom stress, bottom pressure must vary along the contours in a manner determined by wind stress. The resulting bottom pressure field will in general imply the presence of geostrophic flows at the bottom, which is inconsistent with the slippery boundary assumption. This aspect of the analysis leads us to consider the connection to distant forcing, and hence to open-ocean dynamics, for which we must abandon the assumption of constant f. This scenario will be considered further in the next section.

Finally, the assumption that the bottom flow can be shut down relies on there being sufficient stratification. Advection of denser water up or down the slope will tend to reduce the alongshore bottom velocity, but by an amount which depends on the density contrast. For strong currents in weak stratification, it may be impossible to generate sufficient density contrast to shut down the bottom flow. This is the likely to be the case on the inner shelf.

In summary, while the bottom Ekman layer produces an adjustment which tends to reduce the bottom geostrophic flow, there are fundamental reasons why this bottom flow cannot generally shut down. It is required in order to balance the (wind or buoyancy) forcing.

3 The Influence of Ocean Dynamics at the Coast

We have seen above that CTWs propagate rapidly compared to the typical speeds associated with baroclinic open-ocean dynamics. Mode-0 is sufficiently fast that a large-scale adjustment can occur globally in a matter of a few days. Furthermore, low modes also typically propagate at speeds measured in metres per second, and are trapped to the coast with a length scale which is (outside the equatorial waveguide) small compared to ocean basin scales. This disparity in length scales and propagation speeds requires special consideration in both theoretical and numerical models of ocean circulation. A common approach is to use a framework in which the shelf response is assumed to be in a steady equilibrium with the instantaneous ocean interior, effectively assigning an infinite speed to the CTWs.

An example is the quasigeostrophic (QG) approximation, in which sidewalls must be vertical and the CTWs become an infinitely fast series of Kelvin waves. This introduces some subtleties into the boundary conditions, which are resolved by considering volume conservation in each of the ocean's density layers. Once the correct boundary conditions are applied, a boundary-trapped mode is added to the equations enabling the evolution of the ocean circulation to mimic the case with explicitly resolved Kelvin waves (Milliff and McWilliams 1994). This is an unusual case in which the boundary signal has been explicitly considered. It is more usual in idealised ocean circulation studies (such as Stommel 1948; Munk 1950 and their descendants) to solve for the interior circulation plus a western boundary current in a manner which eliminates pressure from the equations, and not to explicitly consider the boundary pressure or sea-level values. Although this is simply a choice of solution method, it does have the effect of obscuring the physics associated with sea level and boundary pressures.

Something similar occurs in the linear shallow water equation approximation used by Johnson and Marshall (2002) to describe the overturning circulation. Again, vertical sidewalls are assumed, with boundary (and equatorial) Kelvin waves travelling fast compared to other time scales. And again, a volume integral constraint is needed to determine the boundary pressure values. By allowing the waves to travel rapidly, causality is obscured, and the entire boundary appears to "know" about the interior ocean simultaneously.

Another system which exhibits similar behaviour is the linear planetary geostrophic equations with topography. Here, wherever the topography is steep enough to produce closed contours of f/h (or, equivalently, of gh/f which we will later show to be a more useful quantity in the sea-level context), it is found that baroclinic signals impinging on the topography can effectively "jump" zonally across the topography, disappearing from one side and appearing more rapidly than expected on the other side, a phenomenon termed a "Rossby wormhole" (Marshall 2011). When the disturbance originates outside the topography, it jumps across from east to west. When it originates inside the topography, as in a basin configuration, the jump is back from west to east, enabling resonant basin modes to occur (as Kelvin waves would do in a vertical sidewall basin). The hidden mechanism involved here is the implicit (infinitely fast) propagation of barotropic topographic Rossby waves around the closed gh/f contours, thus setting up a bottom pressure signal which

absorbs the baroclinic disturbance at one side and re-radiates it on the other side of the topography. Here, the implied boundary waves are barotropic (a limitation of the planetary geostrophic approximation which cannot support Kelvin waves, in which relative vorticity is significant), complementing the baroclinic Kelvin waves of the vertical sidewall case to represent the opposite extreme of the family of CTWs: topographic Rossby waves. Between the quasigeostrophic and planetary geostrophic approximations, we have two illustrations of how CTWs can have a profound effect on ocean adjustment processes, in the baroclinic Kelvin wave limit and the barotropic continental shelf wave limit, respectively.

3.1 Implications of Rapidly Propagating Waves: Smoothing

The implication of these idealised systems is that the continental slope should act as a smoother, taking signals which impinge on it and propagating them rapidly around the boundary. A similar conclusion can be drawn from a scaling argument based on vorticity balance (Hughes et al. 2018). Essentially, if a mesoscale eddy interacts with the sloping seafloor, the lack of flow through the boundary means that horizontal velocities induce vertical velocities at the bottom. However, using the same mesoscale eddy velocity in the vorticity balance results in a much smaller scaling for vertical velocity at the bottom; the vorticity constraint means that the large vertical velocity required by the bottom boundary condition cannot, in fact, be supplied.

As a result, the bottom velocities must be much smaller than typical mesoscale velocities, and the mesoscale is not strongly represented in bottom pressure on the continental slope. In effect, the eddies are "fended off" by the continental slope, although some fluid exchange occurs at scales smaller than the mesoscale; see e.g., Cherian and Brink (2016) for an illustration of this process. Bottom pressures on the slope should therefore be coherent over large distances, in contrast to sea level in the ocean interior which decorrelates rapidly over the mesoscale. The scaling involved here is a reflection of the rapid propagation of CTWs compared to Rossby waves. A related argument can be made in the case of vertical sidewalls as described by Kanzow et al. (2009).

The latest ocean models can now be run with sufficient resolution that it is no longer necessary to artificially smooth the topography to avoid a vertical sidewall, although even at 1/12° resolution, which is still considered high resolution for a global ocean model, the slope remains only marginally resolved in some regions of very steep topography, and details on the slope are certainly not resolved. As a result, it is becoming possible to test these theoretical ideas. It is found that, in a model with realistic mesoscale energy and spectra, the bottom pressure on continental slopes does indeed display coherence over distances measured in tens of thousands of kilometres (Hughes et al. 2018). Using this coherence, it is possible to identify the circuit times for mode-1 and mode-2 CTWs in the (model) North Atlantic as 115 and 205 days, respectively. This defines a time scale with respect to which the system evolution must be "slow" to justify the assumption that CTWs are in equilibrium with the interior (the mode-0 adjustment time is too fast to clearly resolve). The mode-1 time is equivalent to an average CTW speed of around $4–5$ m s^{-1}, significantly faster than the corresponding Kelvin wave speed anywhere in the North Atlantic (Chelton et al. 1998). The fact that the speed is faster than a Kelvin wave speed shows that the finite inclination of the continental slope is an important factor in this boundary adjustment process, so the planetary geostrophic limit (implied barotropic topographic Rossby waves) may be more applicable than the QG limit (implied baroclinic Kelvin waves) over much of the domain.

The model results also confirm the strong suppression of bottom pressure variability amplitude on the continental slope, compared to the mesoscale, and show that the mesoscale spectrum does not penetrate strongly into coastal regions (with the exception of a resonant basin mode in the Caribbean Sea, where the coastal signal has a strong 120-day period excited by mesoscale variability, Hughes et al. 2016). This lack of penetration to the coast is consistent with what is seen in satellite altimetry: sea-level spectra near western boundaries differ strongly between the coast and open ocean, the two regions being typically separated by a minimum of variability near the top of the continental slope (Hughes and Williams 2010; Zhai et al. 2010).

It is worth remarking in this context that small islands are a rather special case. The continental slope smoothing effect is rather ineffective because the slope is closed over relatively small distances, so the mesoscale is only averaged over distances smaller than the mesoscale length scale. For this reason, model diagnostics show little difference between the open-ocean sea level and island coastal sea level, unless the length scales in the open ocean are smaller than the island scale (Williams and Hughes 2013). Thus, the special dynamics at boundaries do not upset the traditional interpretation of island gauges as good sites for monitoring ocean sea-level variations (Woodworth 1991), which is why they have proved so useful for satellite altimeter validation, e.g., Mitchum (1994).

3.2 Oceans with Vertical Sidewalls

Having established that most of the mesoscale variability is filtered out by the continental slope, we are left with the question of the basin-scale variability and how that affects coastal sea level. For many idealised studies, the pressure field (and hence sea level) is implicit in the solution, but is not explicitly shown.

It is helpful first to consider a simple case, for which an explicit solution can easily be found: the linear Munk (1950) or Stommel (1948) two-gyre ocean with vertical sidewalls and constant layer thickness H. Here, we would typically have an eastward wind stress which is maximum at some middle latitude and decays to zero to the north and south. The wind stress curl then excites a cyclonic subpolar gyre on the poleward side (here, sea level falls from east to west, before rising rapidly again across the western boundary current), and an anticyclonic subtropical gyre on the equatorward side (where sea level rises from east to west, before falling across the boundary current). We can sidestep all the vorticity balance arguments, retaining only the information that friction acts dominantly in the western boundary (it is western boundary current friction that balances the alongshore sea-level slope in these models, so this assumption locates that slope on the western rather than eastern boundary), and calculate the coastal sea level simply from the wind stress. Since, when integrating over longitude and depth, there is no net northward transport across any closed section, the effect of the Coriolis force integrates out and the steady, linear, zonal momentum balance (or, strictly, angular momentum about the Earth's axis) becomes a balance between the wind stress and the pressure difference between eastern and western sidewalls:

$$\int_{W}^{E} \tau_s^{(x)} = \int_{-H}^{0} \left(p_E - p_W \right) \mathrm{d}z, \tag{13}$$

where subscripts E and W refer to the eastern and western boundary, and $\tau_s^{(x)}$ is the eastward wind stress (we have neglected sea level in comparison with total open-ocean depth H in the pressure integral). Using the fact that the boundary current is on the west, so pressure on the east is independent of latitude (Hughes and de Cuevas 2001; Hughes et al.

2018), we can subtract off a function of depth only which represents the eastern pressure at any latitude, giving

$$\int_{\text{W}}^{E} \tau_{\text{s}}^{(x)} \, \mathrm{d}x = -H p_{\text{W}}', \tag{14}$$

where p_{W}' is the western boundary pressure minus the reference value at the east. Finally, we can use hydrostatic balance to write $p_{\text{W}}' = \rho_0 g \eta_{\text{W}}$, giving

$$\eta_{\text{W}} = -\frac{1}{\rho_0 g H} \int_{\text{W}}^{E} \tau_{\text{s}}^{(x)} \, \mathrm{d}x, \tag{15}$$

for sea level at the western boundary relative to an assumed constant eastern boundary sea level. The western boundary sea level is therefore lowest between the gyres, at the latitude where the zonally integrated wind stress is strongest.

This pattern can alternatively be understood as the effect of friction in the western boundary currents, which must be flowing down the pressure gradient as they converge towards the intergyre boundary. However, the angular momentum argument is insensitive to details of friction and can even be extended to include nonlinear terms which only become important where there is curvature of the boundary current (Hughes and de Cuevas 2001). In terms of sea level, the final pattern in this simple Munk or Stommel model looks as if the low sea levels of the subpolar gyre are being "advected" towards the equator by CTWs and leaking through the coast in a diluted form somewhat further south (see the middle panels of Fig. 4). This is in fact a good analogy, as we will see.

A simple thermohaline circulation can also be added to this model by assuming that the dynamics discussed above refer to an active layer above a deep, passive abyssal layer. The thermohaline flow is then represented by adding a net northward flow into the active layer, and imagining it to be returned to the south in the abyssal layer. The constant poleward mass transport then does induce a (negative) western sea-level signal via the Coriolis force, and this signal is proportional to f, so it grows in size at higher latitudes.

While the angular momentum argument is pedagogically useful, the real ocean is not in perfect Sverdrup balance and the ocean circulation near to the western boundary can produce more complex patterns than the simple two-gyre solution. However, it has been shown (Minobe et al. 2017) that the linkage between western boundary sea level and sea level at the western end of ocean interior or eastern end of western boundary layer can be understood in the linear limit, by mass conservation, to be given by

$$\eta[x_{\text{W}}(y), y, t] = \frac{f(y)}{f(y_{\text{p}})} \eta[x_{\text{W}}(y_{\text{p}}), y_{\text{p}}, t] + f(y) \int_{y}^{y_{\text{p}}} \frac{\beta}{f^2} \eta[x_{\text{I}}(y'), y', t] \mathrm{d}y', \tag{16}$$

where x_{W} and x_{I} are the zonal positions of the western boundary and western end of the ocean interior, respectively, y_{p} is a reference meridional position that is located poleward of the position y, and $\beta = \mathrm{d}f/\mathrm{d}y$. This equation indicates that the western boundary sea level at a particular latitudinal position y is determined by the coastal sea level at a reference position y_{p} poleward of y, and cumulative effects of ocean interior sea level between y and y_{p}. The physical mechanism is that the mass flux to the western boundary layer due to incident Rossby waves from the ocean interior must be carried by CTWs equatorward. The corresponding meridional transport is well approximated by a current in geostrophic balance, accompanied by a sea-level difference between the western boundary and the ocean interior. The first term on the right-hand side reduces in amplitude in proportion to f on
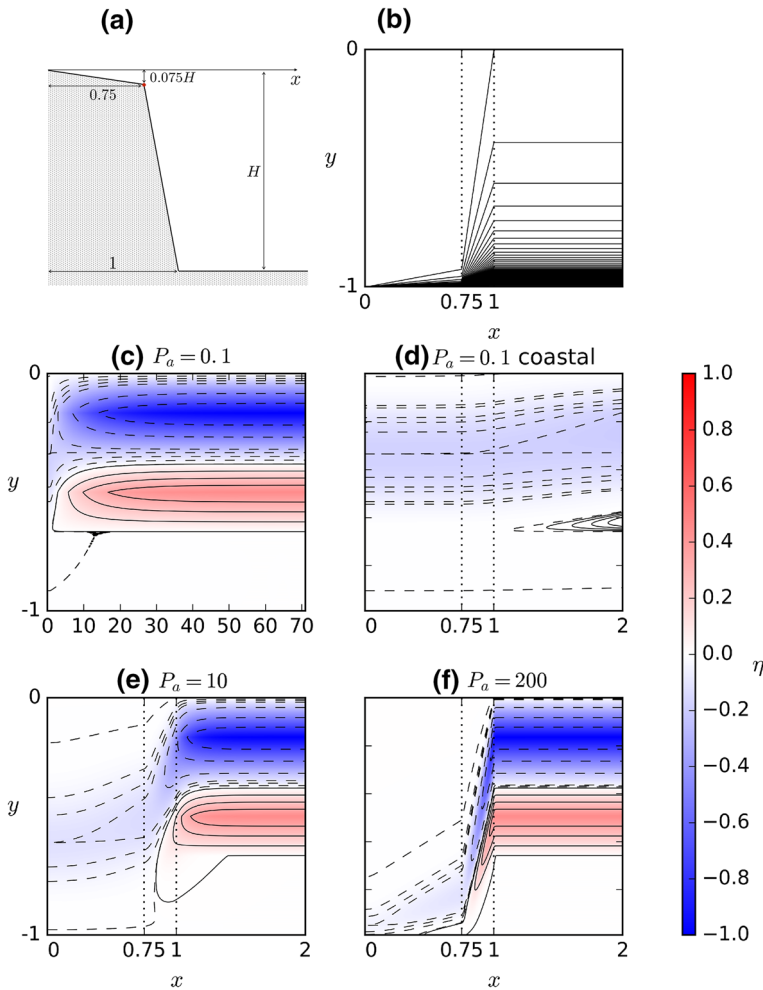
Fig. 4 Western ocean sea level in a barotropic model with topography, adapted from Figs. 3, 4 and 5 of Wise et al. (2018). **a** Geometry of the western boundary topography, with x measured in units such that the foot of the continental slope is at $x = 1$. **b** Corresponding contours of the string function gh/f, with equal spacing (values increase to the south). The y-axis represents a range of 6000 km from the equator at $y = -1$ to the northern boundary at $y = 0$, on this constant-beta geometry. **c** High friction solution, similar to the vertical sidewall case, resolving the full width of the Stommel boundary layer (P_a is the width of the topography measured in units of Stommel boundary layer width). **d** Blow-up of **c**, focusing on the region with topography. **e**, **f** similar to **d**, but with lower friction (narrower Stommel boundary layers)

approaching the equator, reflecting the smaller sea-level signal needed for the same transport to occur at lower latitudes.

The relation (16) is derived for a single-layer linear model, but based on a decomposition into vertical modes, and given the absence of ocean depth in (16), it is suggested that the relation can be used for sea level itself without knowing the detailed vertical mode structures. An important feature of (16) is that the relative importance between the first and second terms are strongly dependent on latitude, because of the aforementioned latitudinal

dependency of the Rossby-wave speed. In lower latitudes, where Rossby waves are fast, interior sea level contributes more strongly than in higher latitudes, and vice versa. That is, the insulation of coastal sea level from the ocean interior sea level is stronger in higher latitudes than in lower latitudes. Hence, in mid-latitudes and high latitudes, the contributions of western boundary sea level at a higher latitude propagating equatorward due to CTWs are generally important. Consistently with this, it is suggested that the projected future sea-level rise seen in coupled climate models between the end of the twentieth century and the end of the twenty-first century in northeast North America, known as a sea-level rise hot spot, is strongly related to the sea-level rise in the Labrador Sea (Minobe et al. 2017).

The results of Minobe et al. (2017) as summarised by Eq. (16) are entirely compatible with the angular momentum argument expressed in Eq. (15). The same western boundary sea level can be derived directly from some assumed wind stress, and the interior sea level can also be so calculated if it is considered to be determined by Sverdrup balance from the same wind stress. These interior and boundary sea levels are then found to be consistent with Eq. (16) (Wise et al. 2018).

3.3 Oceans with Topography

The above results for the vertical sidewall ocean are a rather special case, as can be seen from the dependence of Eq. (15) on the constant depth H. The angular momentum balance relies on knowing the vertical extent of the pressure perturbation on the "sidewalls" of the ocean. When there is a continental slope, currents can flow in different directions over different ocean depths leading to a distribution of "sidewall pressure" which can no longer be calculated based on independent vertical modes, and thus complicating the relationship between the open-ocean circulation and the coastal sea level. At the simplest level, the more surface-intensified the circulation becomes, the smaller the effective H, and hence the larger the associated coastal sea-level signal. However, reversals in the flow can complicate the relationship further, making it questionable whether a meaningful value of H can be determined.

3.4 A Linear, Barotropic Case

An investigation of the simplest (linear, single layer) version of the problem with topography (Wise et al. 2018) has proved revealing. The problem can be reduced to an analogous "advection-diffusion" problem in which a source of water (either a literal source, or the convergence of the Ekman flux due to wind stress) causes a rise in sea level which then behaves as if it is "advected" along characteristics (we use quotation marks to denote words used to describe the analogous problem, it is not a literal advection), while being "diffused" (blurred) by the action of bottom friction. The characteristics in this case are contours of gh/f as shown in Fig. 4b for the bathymetry illustrated in Fig. 4a. These contours can be thought of as the streamfunction responsible for the "advection", so the speed of "advection" is given by the size of the gradient of gh/f, and directed perpendicular to that gradient (along the contours at a speed inversely proportional to their spacing). This "advection" speed was first described by Tyler and Käse (2000) who coined the term "string function" for gh/f to avoid confusion with a true stream function associated with currents. In the constant-slope, f-plane case this "advection" becomes simply a constant speed along the coast, leading to the Arrested Topographic Wave interpretation in which diffusion to the coast happens over "time", but "time" is actually distance along the coast

in the direction of CTW propagation. A similar analogy, expressed in terms of streamfunction rather than bottom pressure or sea level, was exploited by Welander (1968) and Becker and Salmon (1997) giving similar results, although it is much harder to extract information about coastal sea level from this formulation.

In this interpretation, sea level is "advected" westwards in the flat-bottomed ocean interior (at the long Rossby-wave speed) until it encounters the continental slope, whereupon the "advection" turns equatorward and accelerates, due to the convergence of characteristics (string function contours), carrying the sea-level pattern with it. This is a natural extension of the Arrested Topographic Wave concept which allows for a dynamical connection between the open ocean and the coast to be made. Note that, although we are here considering a steady state, this only implies that variation in time is slow compared to the relatively short time taken to establish the coastal response by propagation of CTWs.

In the small friction limit, this "advection-diffusion" balance results in all the diffusion occurring close to the equator, where all gh/f contours converge at the western coast, and no sea-level signal penetrates to the coast. Figure 4f shows a case approaching this limit. This is an unrealistic limit: not only does it assume unrealistically small friction, it also assumes the flow can remain barotropic and coastally trapped right to the equator, which is far from the case with realistic stratification. However, as friction increases (other panels in Fig. 4), penetration of the interior signal to the coast increases and occurs further from the equator. The largest and most rapid penetration (meaning with least southward deflection) occurs in the limit of high friction or narrow continental shelf and slope (these are equivalent limits) and coincides with the vertical sidewall result of Minobe et al. (2017).

The physics of these solutions can be usefully considered in terms of the balance (11). Far offshore, the bottom stress term can be neglected (we ignore local wind stress in this boundary problem), and the alongshore pressure gradient is balanced by a depth-integrated onshore (say) geostrophic flow. Close to the coast, the depth-integrated flow becomes negligible and the balance is between the pressure gradient and the bottom stress. This is the same switch from geostrophic to frictional balance that occurs in damped CTWs. Between these two limits, either the bottom stress must build up to provide an offshore Ekman flux which balances the onshore geostrophic flow, or the pressure gradient must reduce as the geostrophic flow is deflected along the slope. In the former case, there is "diffusion" of the sea-level signal across gh/f contours, and a coastal response appears. In the latter case, there is no "diffusion", and no coastal response. This interpretation explains an apparent contradiction with Csanady (1978), who found that all the open-ocean signal would eventually make it to the coast for long enough wavelengths. In that study (with constant f), the depth-integrated onshore flow was always taken to be zero (consistent with the design of the Arrested Topographic Wave to model circulation over the inner shelf), meaning that the geostrophic onshore flow was always balanced by an offshore flow in the bottom Ekman layer, and a connection with the open ocean (where the pressure gradient is not balanced by bottom stress) was not truly made.

Thus, the size and position of the coastal signal depend on both friction and the shape of the boundary topography. This conclusion is consistent with Higginson et al. (2015), who found that the northward drop in U.S. Atlantic coastal sea level was much smaller and further south than the interior ocean signal, as the above discussion would suggest. They also found that different ocean models disagreed as to the extent of this southward deflection, with some showing much more of a step near Cape Hatteras than would be suggested by the observations, which show almost all the step in south Florida. This is suggestive of the kind of sensitivity to details of topography and friction that the linear barotropic model indicates should be expected.

Further analytical work on the linear barotropic model (Wise et al. 2019) has shown that certain features are robust. The western boundary coastal signal can always be computed as a weighted integral of the open-ocean signal from poleward of the point in question just as in the vertical sidewall case as expressed in Eq. (16), but the weightings of the interior and poleward sea-level signals become different from those in (16). The weighted integral can also still be interpreted as a series of damped boundary modes which propagate information towards the equator. The idea that the interior signal is carried equatorward by CTWs while being leaked across the slope by bottom friction (Huthnance 1987, 2004) is therefore a useful interpretation of the dynamics.

It should be noted, however, that the coastal modes in this interpretation can become somewhat more complicated than conventional f-plane CTWs. If f is allowed to vary, a new time scale is introduced, which is the shortest period at which Rossby waves can exist. This period is given by $4\pi/\beta L_\mathrm{d}$. Using $L_\mathrm{d} = c/|f|$ where c is the gravity wave speed for the same vertical mode, and approximating c as about 2.5 m s^{-1} for the first baroclinic mode (Chelton et al. 1998), this can be approximated as $T \approx |\tan\phi|$ where T is measured in years and ϕ is latitude (although near the poles, the separation of variables used to derive the standard Rossby-wave dispersion relation no longer applies). For a truly barotropic mode, taking $c \approx 200$ m s^{-1}, the critical period T is 80 times shorter. The few early studies of CTWs which allowed for variations in f, e.g., Allen and Romea (1980), Grimshaw (1977), limited the frequency range to exclude Rossby waves. When Rossby waves are possible, energy can leak away from the boundaries as short Rossby waves from the west, or long Rossby waves from the east. As shown in the vertical sidewall case by Marshall and Johnson (2013), this results in the boundary signals transitioning from Kelvin to Rossby waves, or to Munk (1950) or Stommel (1948) boundary layers as friction becomes important. More work is needed to understand the implications of this, but initial work (Wise et al. 2019) suggests that the general conclusions carry over to the case with topography, suggesting that great care needs to be exercised in the interpretation of measurement of signals propagating along boundaries, as phase speeds can be quite different from those seen in f-plane or higher frequency CTWs.

Nonetheless, the linear barotropic model does show that signals generated in the interior are "advected" to the west at the long Rossby-wave speed, and then along gh/f countours along the boundary at a speed which can be considered to be the relevant CTW speed, while being "diffused" by bottom friction.

3.5 Considerations of Nonlinearity

The model considered above remains highly simplified, being linear and with only rudimentary stratification (although barotropic, the open-ocean part of this model can also be thought of as a model with a single active layer above a passive abyss) There are hints that nonlinear effects may produce a richer array of behaviours on western boundaries, including the formation of fronts in boundary pressure, and hence in sea level. The essential mechanism is the overwhelming of CTW propagation by the flow itself, leading to a reversal of the characteristic velocity along part of the boundary (such reversals of characteristic velocity also lie at the heart of longstanding questions of the extent to which western boundary currents can be considered to be passive in ocean thermocline theory). The flow must oppose the wave propagation to achieve this reversal, implying that the reversal is in the subtropical gyre region (the Gulf Stream in the North Atlantic). In a vertical sidewall case, the relevant waves are Kelvin waves which, at least for high enough modes, can

certainly be halted by realistic boundary currents. Loss of balance (generation of small-scale gravity waves which remove energy from the "balanced" part of the flow which can be determined from the potential vorticity equation) is found to occur at the point of convergence of opposing characteristic velocities at the boundary, leading to formation of fronts there (Dewar and Hogg 2010; Deremble et al. 2017). This mechanism was sketched out (in a case with sloping topography modelled on the Gulf Stream geometry) by Stern (1998) and has gained qualitative support from model sensitivity studies (Schoonover et al. 2017), in which CTW speeds are compared with current speeds to suggest the plausibility of this mechanism as an explanation of Gulf Stream separation.

Nonlinear behaviour may, in fact, arise even without the nonlinear terms in the momentum equations. It has proved possible to solve a variety of special cases of the planetary geostrophic equations with sloping boundaries, and these also show a rich variety of behaviours with the formation of fronts, and recirculations either side of the boundary current extension (Salmon 1994; Ford 2000). Again, these solutions can be considered in terms of characteristic "velocities", "advecting" the dynamical quantities, coupled with a form of "diffusion". These "velocities" are compounded of a westward component associated with the baroclinic Rossby-wave speed, a component along the topography in the direction of CTW propagation, a genuine advection by the flow, and a modification of the Rossby-wave speed due to finite deformation of the stratification (particularly strong in the subpolar gyre). In several cases, the characteristic "velocity" at the western boundary is found to be polewards in the equatorward part of the subtropical gyre, converging with an equatorward velocity from the subpolar gyre, and forming a front at the convergence [a little further offshore the front is found much further polwards, see figures 5–7 of Salmon (1994)]. This suggests the possibility of sharp steps in coastal sea level mediated by this competition between advection by the flow and "advection" by CTWs, although the "advected" quantity in these more complex solutions is no longer as simple as the bottom pressure. This is an area ripe for further exploration, with potentially important consequences for understanding and predicting coastal sea level.

3.6 Eastern Boundaries

The above has focused on western boundaries, where the dynamics are rather complicated. At eastern boundaries things are more straightforward. The open-ocean characteristic "velocities" near to eastern boundaries are dominated by the westward Rossby-wave speed except at the equator where the influence of the eastward-propagating equatorial Kelvin and Yanai waves is felt. Along the boundary, the CTWs propagate away from the equator, so all coastal signals should either propagate from the equator, or be generated by local forcing close to the coast. The vertical sidewall analytical models suggest that the signal propagating from the equator would, on time scales longer than the basin circuit time, be determined by the layerwise mass balance constraint.

Model diagnostics are consistent with this interpretation (Hughes et al. 2018). They show that, below about 200 m, the bottom pressure variations propagate away from the equator at speeds typical of CTWs, becoming at interannual time scales almost uniform along the entire eastern boundary, and very small (less than 1 cm of water). Variations in sea level along the eastern boundary (and they do occur) must therefore be generated either from equatorial sources or by shelf sea dynamics, with some of the effects radiating out into the open ocean. Illustrating this, it is found that regional model simulations of the US Pacific coast perform better when using "clamped" boundary conditions to the south,

directly importing the observed properties at that boundary via a data assimilating global model, as opposed to the "radiation plus nudging" conditions applied at other boundaries (Durski et al. 2015). Both boundary wave propagation and local winds play important roles in the coastal sea level in this region (Kurapov et al. 2017). The radiation of Rossby waves has been suggested as a mechanism for the formation of poleward-flowing undercurrents below the equatorward winds on certain boundaries (Samelson 2017), an example of the coastal variability influencing the open ocean rather than vice versa.

4 Conclusions

The interaction between open ocean and the coast is a subtle issue, especially at western boundaries. We have found that it is possible to think of CTWs as effectively advecting sea level (or bottom pressure) signals rapidly along the continental slope, in the direction of CTW propagation, with bottom friction acting to diffuse the signal slowly across the slope. Thus the coastal sea-level signal emerges from the balance between these two processes and can become very small when bottom friction is small. The sea-level signals reach the continental slope as a result of a similar Rossby-wave "advection" from east to west in much of the ocean, or a Kelvin wave "advection" to the east at the equator. Thus eastern boundary coastal sea-level signals are only influenced by the equatorial open ocean, as well as near-coastal direct forcing. The western boundary coastal sea level, on the other hand, is influenced by the open ocean from all latitudes.

The conventional vertical sidewall case appears to produce the largest western boundary coastal signals, which are still significantly smaller than the associated open-ocean signals, and displaced towards the equator. More realistic topography and lower bottom friction act to reduce the size of these signals further, and push them further towards the equator. Thus, it is expected that western boundary coastal signals should be smaller than interior ocean signals and should smooth those interior signals over long distances (greatly reducing the influence of mesoscale variability). In the linear limit, western boundary coastal sea level should only be affected by ocean signals poleward of the latitude being considered.

Nonlinear effects, however, may be very important, permitting an advective influence of open-ocean sea level from equatorward of the coastal point, associated with poleward-flowing western boundary currents. Sharp steps along western boundaries may be a manifestation of the convergence of this propagation of influence from poleward (by CTWs) and equatorward (by western boundary currents). More work is needed to clarify these issues.

The smoothing and the equatorward "advection" of open-ocean sea-level signals, both of which act to reduce the magnitude of the signal, only apply when the continental slope is long and spans a wide latitude range. In the case of small islands, the smoothing is limited to the length of the depth contours which close around the island, and the equatorward displacement is similarly limited. This means that the open-ocean influence is felt much more strongly at small islands, increasing the risks from sea-level change, but also meaning that measurements from tide gauges on small islands are representative of the surrounding ocean, in contrast to the case for, especially extratropical, continental tide gauges.

For all cases, it should be stressed that we have here considered only the dynamical component of sea-level change, which results in the sea surface not being level. On top of this component, any increase in the volume of water in the ocean will transmit freely to the coast, with a distribution depending purely on the response of the solid Earth and its gravity field to the redistribution of mass, as considered elsewhere in this volume. In addition,

we have ignored the inverse barometer response to atmospheric pressure changes, which would also be felt at the coast just as strongly as in the open ocean.

References

Andersen OB, Nielsen K, Knudsen P, Hughes CW, Bingham R, Fenoglio-Marc L, Gravelle M, Kern M, Padilla Polo S (2018) Improving the coastal mean dynamic topography by geodetic combination of tide gauge and satellite altimetry. Mar Geod 41(6):517–545. https://doi.org/10.1080/01490419.2018.1530320

Allen JS, Romea RD (1980) On coastal trapped waves at low latitudes in a stratified ocean. J Fluid Mech 98:555–585

Becker JM, Salmon R (1997) Eddy formation on a continental slope. J Mar Res 55:181–200

Bingham RJ, Hughes CW (2012) Local diagnostics to estimate density-induced sea level variations over topography and along coastlines. J Geophys Res 117(C1):C01013. https://doi.org/10.1029/2011JC007276

Brink KH (1982) The effect of bottom friction on low-frequency coastal trapped waves. J Phys Oceanogr 12:127–133

Brink KH (1991) Coastal trapped waves and wind-driven currents over the continental shelf. Annu Rev Fluid Mech 23(1991):389–412

Calafat FM, Chambers DP, Tsimplis MN (2012) Mechanisms of decadal sea level variability in the eastern North Atlantic and the Mediterranean Sea. J Geophys Res Oceans 117:C09022. https://doi.org/10.1029/2012JC008285

Calafat FM, Chambers DP, Tsimplis MN (2013) Inter-annual to decadal sea-level variability in the coastal zones of the Norwegian and Siberian Seas: the role of atmospheric forcing. J Geophys Res Oceans 118:1287–1301. https://doi.org/10.1002/jgrc.20106

Chelton DB, Schlax MA (1996) Global observations of oceanic Rossby waves. Science 272:234–238

Chelton DB, de Szoeke RA, Schlax MA, El Naggar K, Siwertz N (1998) Geographical variability of the first baroclinic Rossby radius of deformation. J Phys Oceanogr 28:433–460

Cherian DA, Brink KH (2016) Offshore transport of shelf water by deep-ocean eddies. J Phys Oceanogr 46:3599–3621. https://doi.org/10.1175/JPO-D-16-0085.1

Csanady GT (1978) The arrested topographic wave. J Phys Oceanogr 8:47–62

Csanady GT (1982) Circulation in the coastal ocean, vol 2. Springer, Dordrecht, p 279

Deremble B, Johnson ER, Dewar WK (2017) A coupled model of interior balanced and boundary flow. Ocean Model 119:1–12. https://doi.org/10.1016/j.ocemod.2017.09.003

Dewar WK, Hogg A (2010) Topographic inviscid dissipation of balanced flow. Ocean Model 32:1–13. https://doi.org/10.1016/j.ocemod.2009.03.007

Dale A, Huthnance JM, Sherwin TJ (2001) Coastal trapped internal waves and tides at near-inertial frequencies. J Phys Oceanogr 31(10):2958–2970

Durski SM, Kurapov AL, Allen JS, Kosro PM, Egbert GD, Shearman RK, Barth JA (2015) Coastal Ocean variability in the US Pacific Northwest region: seasonal patterns, winter circulation, and the influence of the 2009–2010 El Niño. Ocean Dyn 65(12):1643–1663. https://doi.org/10.1007/s10236-015-0891-1

Enfield DB, Allen JS (1980) On the structure and dynamics of monthly mean sea level anomalies along the Pacific coast of North and South America. J Phys Oceanogr 10:557–578. https://doi.org/10.1175/1520-0485(1980) 010<0557:OTSADO>2.0.CO;2

Ford R (2000) A baroclinic western boundary current over a continental slope. J Mar Res 58(3):327–373

Fukumori I, Wang O, Llovel W, Fenty I, Forget G (2015) A near-uniform fluctuation of ocean bottom pressure and sea level across the deep ocean basins of the Arctic Ocean and the Nordic Seas. Prog Oceanogr 134:152–172. https://doi.org/10.1016/j.pocean.2015.01.013

Gill AE (1982) Atmosphere-ocean dynamics, International geophysics series, 30. Academic Press, Cambridge

Gregory JM, Griffies SM, Hughes CW, Lowe JA, Church JA, Fukumori I, Gomez N, Kopp RE, Landerer F, Ponte RM, Stammer D, Tamisiea ME, van de Wal RS Concepts and terminology for sea level—mean, variability and change, both local and global. Surv Geophys (this volume)

Grimshaw R (1977) The effects of a variable Coriolis parameter, coastline curvature and variable bottom topography on continental-shelf waves. J Phys Oceanogr 7:547–554

Higginson S, Thompson KR, Woodworth PL, Hughes CW (2015) The tilt of mean sea level along the east coast of North America. Geophys Res Lett 42(5):1471–1479. https://doi.org/10.1002/2015GL063186

Hughes CW (2008) A form of potential vorticity equation for depth-integrated flow with a free surface. J Phys Oceanogr 38:1131–1136

Hughes CW, de Cuevas BA (2001) Why western boundary currents in realistic oceans are inviscid: a link between form stress and bottom pressure torques. J Phys Oceanogr 31(10):2871–2885. https://doi.org/10.1175/1520-0485(2001)031%3C2871:WWBCIR%3E2.0.CO;2

Hughes CW, Meredith MP (2006) Coherent sea-level fluctuations along the global continental slope. Philos Trans R Soc Lond A 364(1841):885–901. https://doi.org/10.1098/rsta.2006.1744

Hughes CW, Williams SDP (2010) The color of sea level: importance of spatial variations in spectral shape for assessing the significance of trends. J Geophys Res 115(C10):C10048. https://doi.org/10.1029/2010JC006102

Hughes CW, Williams Joanne, Coward AC, de Cuevas BA (2014) Antarctic circumpolar transport and the southern mode: a model investigation of interannual to decadal time scales. Ocean Sci 10:215–225. https://doi.org/10.5194/os-10-215-2014

Hughes CW, Bingham RJ, Roussenov V, Williams Joanne, Woodworth PL (2015) The effect of Mediterranean exchange flow on European time mean sea level. Geophys Res Lett 42(2):466–474. https://doi.org/10.1002/2014GL062654

Hughes CW, Williams Joanne, Hibbert A, Boening C, Oram J (2016) A Rossby whistle: a resonant basin mode observed in the Caribbean Sea. Geophys Res Lett 43:7036–7043. https://doi.org/10.1002/2016GL069573

Hughes CW, Williams Joanne, Blaker A, Coward A, Stepanov V (2018) A window on the deep ocean: the special value of ocean bottom pressure for monitoring the large-scale, deep-ocean circulation. Prog Oceanogr 161:19–46. https://doi.org/10.1016/j.pocean.2018.01.011

Huthnance JM (1978) On coastal trapped waves: analysis and numerical calculation by inverse iteration. J Phys Oceanogr 8:74–92

Huthnance JM (1987) Effects of longshore shelf variations on barotropic continental shelf waves. Prog Oceanogr 19:177–220

Huthnance JM (2001) Coastal trapped waves. In: Steele JH, Thorpe SA, Turekian KK (eds) Encyclopedia of ocean sciences. Academic Press, San Diego, pp 489–496

Huthnance JM (2004) Ocean-to-shelf signal transmission: a parameter study. J Geophys Res 109:C12029. https://doi.org/10.1029/2004JC002358

Huthnance JM, Mysak LA, Wang DP (1986) Coastal trapped waves. In: Mooers CNK (ed) Coastal and Estuarine sciences 3: Baroclinic processes on continental shelves. American Geophysical Union, Washington, pp 1–18

Johnson HL, Marshall DP (2002) A theory for the surface Atlantic response to thermahaline variability. J Phys Oceanogr 32:1121–1132

Kanzow T, Johnson HL, Marshall DP, Cunningham SA, Hirschi JJM, Mujahid A, Bryden HL, Johns WE (2009) Basinwide integrated volume transports in an eddy-filled ocean. J Phys Oceanogr 39:3091–3109. https://doi.org/10.1175/2009JPO4185.1

Kurapov AL, Erofeeva SY, Myers E (2017) Coastal sea level variability in the US West Coast Ocean Forecast System (WCOFS). Ocean Dyn 67:23–36. https://doi.org/10.1007/s10236-016-1013-4

LaCasce JH (2017) The prevalence of oceanic surface modes. Geophys Res Lett 44:11097–11105. https://doi.org/10.1002/2017GL075430

Lin H, Thompson KR, Huang J, Veronneau M (2015) Tilt of mean sea level along the Pacific coasts of North America and Japan. J Geophys Res Oceans 120:6815–6828. https://doi.org/10.1002/2015JC010920

Lorbacher K, Marsland SJ, Church JA, Griffies SM, Stammer D (2012) Rapid barotropic sea level rise from simulated ice-sheet melting scenarios. J Geophys Res 117:C06003. https://doi.org/10.1029/2011JC007733

MacCready P, Rhines PB (1993) Slippery bottom boundary layers on a slope. J Phys Oceanogr 23:5–22

Marshall DP (2011) Rossby wormholes. J Mar Res 69:309–330

Marshall DP, Johnson HL (2013) Propagation of meridional circulation anomalies along western and eastern boundaries. J Phys Oceanogr 43:2699–2717

Milliff RF, McWilliams JC (1994) The evolution of boundary pressure in ocean basins. J Phys Oceanogr 24:1317–1338

Minobe S, Terada M, Qiu B, Schneider N (2017) Western boundary sea level: a theory, rule of thumb, and application to climate models. J Phys Oceanogr 47(5):957–977

Mitchum G (1994) Comparison of TOPEX sea surface heights and tide gauge sea levels. J Geophys Res 99(C12):24541–24553

Munk WH (1950) On the wind-driven ocean circulation. J Meteorol 7:79–93

Mysak LA (1980) Topographically trapped waves. Annu Rev Fluid Mech 12:45–76

Mysak LA (1980) Recent advances in shelf wave dynamics. Rev Geophys Space Phys 18:211–241

Rhines PB (1970) Edge, bottom and Rossby waves. Geophys Fluid Dyn 1:273–302

Rio M-H, Mulet S, Picot N (2014) Beyond GOCE for the ocean circulation estimate: synergetic use of altimetry, gravimetry, and in situ data provides new insight into geostrophic and Ekman currents. Geophys Res Lett 41:8918–8925. https://doi.org/10.1002/2014GL061773

Salmon R (1994) Generalized two-layer models of ocean circulation. J Mar Res 52:865–9082

Samelson RM (2017) Time-dependent linear theory for the generation of poleward undercurrents on eastern boundaries. J Phys Oceanogr 47:3037–3059. https://doi.org/10.1175/JPO-D-17-0077.1

Schoonover J, Dewar WK, Wienders N, Deremble B (2017) Local sensitivities of the Gulf Stream separation. J Phys Oceanogr 47:353–373. https://doi.org/10.1175/JPO-D-16-0195.1

Stern M (1998) Separation of a density current from the bottom of a continental shelf. J Phys Oceanogr 28:2040–2049. https://doi.org/10.1175/1520-0485(1998)028%3C2040:SOADCF%3E2.0.CO;2

Stommel H (1948) The westward intensification of wind-driven ocean currents. Trans Am Geophys Union 29:202–206

Tyler RH, Käse R (2000) A "string function" for describing the propagation of large-scale energy anomalies in a rotating fluid. Geophys Astrophys Fluid Dyn 92:31–64

Welander P (1968) Wind-driven circulation in one- and two-layer oceans of variable depth. Tellus 20:1–15

Williams Joanne, Hughes CW (2013) The coherence of small island sea level with the wider ocean: a model study. Ocean Sci 9:111–119. https://doi.org/10.5194/os-9-111-2013

Wise A, Hughes CW, Polton J (2018) Bathymetric influence on the coastal sea level response to ocean gyres at western boundaries. J Phys Oceanogr 48:2949–2964. https://doi.org/10.1175/JPO-D-18-0007.1

Wise A, Hughes CW, Polton J, Huthnance JM (2019) Leaky slope waves: unusual consequences of the beta-effect along western boundaries with bottom topography and dissipation. J Phys Oceanogr (submitted)

Woodworth PL (1991) The permanent service for mean sea level and the global sea level observing system. J Coast Res 7(3):699–710

Woodworth PL, Hughes CW, Bingham RJ, Gruber T (2012) Towards worldwide height system unification using ocean information. J Geod Sci 2(4):302–318. https://doi.org/10.2478/v10156-012-0004-8

Zhai X, Johnson HL, Marshall DP (2010) Significant sink of ocean-eddy energy near western boundaries. Nat Geosci 3:609–612

Affiliations

Chris W. Hughes[1,2] · Ichiro Fukumori[3] · Stephen M. Griffies[4] · John M. Huthnance[2] · Shoshiro Minobe[5] · Paul Spence[6] · Keith R. Thompson[7] · Anthony Wise[1,2]

[1]   Department of Earth, Ocean and Ecological Sciences, University of Liverpool, Jane Herdman Building, 4 Brownlow Street, Liverpool L69 3GP, UK

[2]   National Oceanography Centre, 6 Brownlow Street, Liverpool L3 5DA, UK

[3]   Jet Propulsion Laboratory, California Institute of Technology, 4800 Oak Grove Dr, Pasadena, CA 91109, USA

[4]   NOAA Geophysical Fluid Dynamics Laboratory, Princeton University Program in Atmospheric and Oceanic Sciences, Princeton University Forrestal Campus, 201 Forrestal Road, Princeton, NJ 08540-6649, USA

[5]   Department of Earth and Planetary Sciences, Faculty of Science, Hokkaido University, N10, W8, Kita-ku, Sapporo 060-0810, Japan

[6]   Climate Change Research Centre, University of New South Wales, Level 4, Mathews Building, Sydney, NSW 2052, Australia

[7]   Department of Oceanography, Dalhousie University, LSC, Room 3631, 1355 Oxford Street, PO BOX 15000, Halifax, NS B3H 4R2, Canada